Optimally Pre-Damped Switched-Inductor Piezoelectric Energy-Harvesting Charger

Siyu Yang, *Graduate Student Member, IEEE,* and Gabriel A. Rincon-Mora *Fellow, IEEE*
Georgia Institute of Technology, Atlanta, Georgia 30332-0250 U.S.A.
E-mail: jimsyyang@gatech.edu and Rincon-Mora@gatech.edu

***Abstract*—Wireless microsensors in factories, hospitals, cars, and so on process information that can save money, energy, and lives. Unfortunately, tiny batteries exhaust quickly, and replacing so many of them frequently is impractical. This is why recharging them with ambient energy is so appealing, especially when vibrations, for example, are abundant and steady. Still, tiny piezoelectric transducers draw so little power that they hardly damp motion. Luckily, pre-damping the transducer draws more power. This paper shows that symmetrical and asymmetrical pre-damping strategies draw the same power, but of the two, the proposed symmetrical case consumes less energy and therefore outputs more power. With this approach, the proposed system consumes 82% less power and generates 7.8× more output power.**

Keywords—Switched-inductor charger, piezoelectric harvester, transducer, damping, ambient kinetic energy, vibrations, motion.

I. Motion-Powered Microsystems

Wireless microsystems networked across factories, hospitals, homes, cars, and so on sense, share, and process information that can save money, energy, and lives [1]. Unfortunately, their tiny batteries exhaust quickly. And replacing thousands of batteries across a network is impractical, costly, and oftentimes impossible. This is one driving factor why drawing power from the environment is so appealing today.

Although transducers output over 100× more power from sunlight than from artificial lighting and other sources [2], sunlight is seldom available. Luckily, engine vibrations and motion, which at 100–300 $\mu W/cm^3$ generate the next highest power levels, are abundant and steady in many applications [3]. Tiny transducers, however, draw a miniscule fraction of the energy available, so they hardly damp motion, and as a result, generate very little power.

A harvester, therefore, cannot on its own supply the needs of a microsystem adequately. This is why energy-harvesting microsensors like the one Fig. 1 exemplifies normally use a harvesting charger to continually replenish a battery v_{BAT} that a power-supply circuit can tap to energize system components. This way, the harvester charges v_{BAT} while the system idles. And when v_{BAT} garners sufficient energy, the power-supply circuit wakes to energize the sensor, processor, and power amplifier that sense, process, and transmit information.

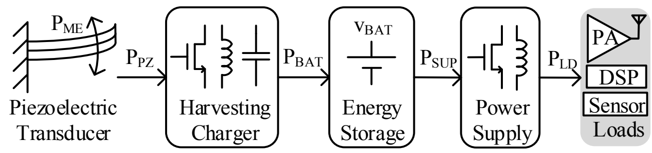

Fig. 1. Motion-powered wireless microsensor system.

The harvesting charger should draw lots of power while itself consuming little. In the state of the art, recycling bridges draw the most power [4]. Unfortunately, they require one inductor for recycling energy between half cycles, one capacitor to continually draw charge at the highest possible voltage, and a switched-inductor circuit to steer drawn power into v_{BAT} [5]. So not only do two inductors and one capacitor occupy board space but also more switches dissipate power.

Although bridgeless switched-inductor harvesters draw less power, they require only one inductor and four switches [6]. Plus, pre-damped solutions draw and deliver more power, but only to the extent that integration limits discussed in Section II allow. To understand these constraints, Section III describes how switched-inductor harvesters draw power. Sections IV, V, and VI then introduce and compare damping strategies and proposes a solution that dissipates less energy and delivers more power. Section VII ends with conclusions.

II. Effects of Miniaturization

A. Piezoelectric Transducer

The charge that motion produces when bending a piezoelectric material is proportional to displacement. Tiny cantilevers, however, hardly displace and only draw a very small fraction of the kinetic energy available. As a result, drawing power inflicts negligible effects on displacement. This means, damping effects are miniscule and the coupling factor between the mechanical and electrical domains is very low [7].

Since drawing power barely damps small piezoelectric transducers, they behave like ideal alternating Norton-equivalent current sources i_{PZ} [8]. Piezoelectric power P_{PZ} is therefore proportional to i_{PZ} and the voltage v_{PZ} across the capacitance C_{PZ} that the structure exhibits. So since P_{PZ} rises with v_{PZ} without affecting i_{PZ}, energy-harvesting chargers should keep v_{PZ} as high as possible to draw more power.

B. Switched Inductor

Harvesting chargers use inductors to transfer energy because the mV's that their switches drop consume little power [9]. To keep these losses as low as possible, an inductor L_X should carry more energy $0.5L_Xi_L^2$ with less current i_L. For this, L_X should be high, and as a result, so should the number of turns and cross-sectional area of the winding [10].

For volts to induce no more than mA within µs, L_X should be hundreds of µH. The winding must therefore incorporate many turns, which in small form factors only a thin coil can accommodate. Unfortunately, because thinner coils are more resistive, the equivalent series resistance R_{ESR} of tiny off-chip 100–500-µH inductors is typically high at 1–5 Ω [11].

For perspective, CMOS switches dissipate the least power when sized to balance ohmic and gate-drive losses. Modern switches balance these losses when their resistances R_{MOS} are less than 100 mΩ [12]. But since R_{ESR} is so much greater than R_{MOS}, R_{ESR} power overwhelms that of R_{MOS}, and by translation, that of gate drive. So R_{ESR} power P_R normally dominates all other losses to dictate what fraction of piezoelectric power P_{PZ} the battery v_{BAT} ultimately receives.

Capacitor Transfer: Before delivering energy, L_X holds energy $E_{L(PK)}$ with peak inductor current $i_{L(PK)}$. When connected to a capacitor C_X, L_X and C_X exchange $E_{L(PK)}$ every quarter cycle of their resonance period τ_{LC}. Since L_X's i_L is nearly sinusoidal through this time, i_L's root–mean–square (RMS) current is $i_{L(PK)}/\sqrt{2}$. So to transfer $E_{L(PK)}$, L_X's ohmic power $P_{R(C)}$ across vibration period t_{VIB} is a $0.25\tau_{LC}/t_{VIB}$ fraction of RMS power across τ_{LC}, where t_{VIB} is usually long at 1–1000 ms [10]:

$$P_{R(C)} \approx i_{L(RMS)}{}^2 R_{ESR}\left(\frac{\tau_{LC}}{4t_{VIB}}\right) = \left(\frac{i_{L(PK)}}{\sqrt{2}}\right)^2 R_{SER}\left(\frac{2\pi\sqrt{L_X C_X}}{4t_{VIB}}\right). \quad (1)$$

$P_{R(C)}$ therefore climbs with $i_{L(PK)}{}^2$, and since L_X transfers $0.5L_X i_{L(PK)}{}^2$, with L_X's peak energy packet $E_{L(PK)}$.

Partial Capacitor Transfer: C_X's voltage v_C is, like i_L, sinusoidal. So when transferring part of L_X's energy, time t_X lapses the sinusoidal fraction of the resonance period τ_{LC} that v_C requires to reach the $v_{C(X)}$ fraction of peak voltage $v_{C(PK)}$:

$$t_X = \left(\frac{\tau_{LC}}{2\pi}\right)\sin^{-1}\left(\frac{v_{C(X)}}{v_{C(PK)}}\right). \quad (2)$$

Since L_X's energy and i_L peak when C_X's energy and v_C are zero, i_L is the cosine counterpart of v_C:

$$i_L = i_{L(PK)}\cos\left[2\pi\left(\frac{t}{\tau_{LC}}\right)\right]. \quad (3)$$

So to transfer a t_X sinusoidal fraction of L_X's $E_{L(PK)}$ at $i_{L(PK)}$, L_X's ohmic power $P_{R(X)}$ across t_{VIB} is

$$\begin{aligned} P_{R(CX)} &= i_{L(RMS)}{}^2 R_{ESR} = \left[\left(\frac{1}{t_{VIB}}\right)\int_0^{t_X} i_L{}^2\,dt\right]R_{ESR} \\ &= \left(\frac{i_{L(PK)}{}^2}{t_{VIB}}\right)\left\{\frac{t_X}{2} + \left(\frac{\tau_{LC}}{8\pi}\right)\sin\left[4\pi\left(\frac{t_X}{\tau_{LC}}\right)\right]\right\}R_{ESR} \end{aligned}. \quad (4)$$

So like $P_{R(C)}$, $P_{R(CX)}$ climbs with $i_{L(PK)}{}^2$ and L_X's $E_{L(PK)}$.

Battery Transfer: Since L_X's voltage is constant at v_{BAT} when transferring $E_{L(PK)}$ to v_{BAT}, i_L falls linearly to zero across t_{BAT} connection time $L_X i_{L(PK)}/v_{BAT}$. RMS current $i_{L(RMS)}$ across t_{BAT} is therefore $i_{L(PK)}/\sqrt{3}$ and L_X's ohmic power $P_{R(B)}$ across vibration period t_{VIB} is a t_{BAT}/t_{VIB} fraction of RMS power across t_{BAT}:

$$P_{R(B)} \approx i_{L(RMS)}{}^2 R_{ESR}\left(\frac{t_{BAT}}{t_{VIB}}\right) = \left(\frac{i_{L(PK)}}{\sqrt{3}}\right)^2 R_{SER}\left(\frac{L_X i_{L(PK)}}{v_{BAT} t_{VIB}}\right). \quad (5)$$

$P_{R(B)}$ therefore climbs with $i_{L(PK)}{}^3$, which is faster than $P_{R(C)}$ and $P_{R(CX)}$ rise with L_X's peak energy $E_{L(PK)}$.

III. Synchronous Piezoelectric Discharges

A. Basic Half-Cycle Operation

In piezoelectric chargers, the transducer's i_{PZ} charges C_{PZ} across half cycles so that the switched inductor L_X can drain and deliver C_{PZ}'s energy to v_{BAT} between half cycles. This way, like the solid black trace in Fig. 2 shows, i_{PZ} charges C_{PZ} to open-circuit voltage v_{OC} every half cycle. And between half cycles, L_X discharges C_{PZ} and delivers C_{PZ}'s energy $E_{C(PK)}$ at v_{OC} to v_{BAT}. i_{PZ} therefore supplies $E_{PZ(1/2)}$ every half cycle:

$$E_{PZ(1/2)} = E_{C(PK)} = 0.5C_{PZ}v_{OC}{}^2. \quad (6)$$

Notice that the μs time L_X requires to transfer these energy packets is so much shorter than t_{VIB}'s ms period that transfers are nearly instantaneous in the figure.

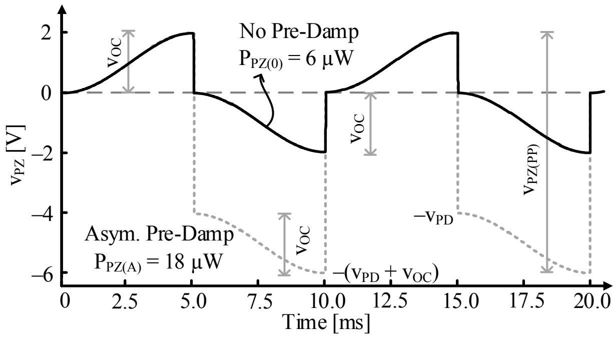

Fig. 2. Basic and asymmetrically pre-damped piezoelectric voltages.

B. Pre-Damped Half-Cycle Operation

Pre-charging C_{PZ} to v_{PD} between half cycles allows v_{PZ} to both start and end at higher voltages. Since i_{PZ} is basically a current source, i_{PZ} delivers more energy this way, with a higher voltage. In other words, v_{PD} raises the piezoelectric damping force against which motion works to supply power.

At 5 ms in Fig. 2, for example, L_X pre-damps C_{PZ} to $-v_{PD}$ and i_{PZ} charges C_{PZ} across i_{PZ}'s negative half cycle another v_{OC} to $-(v_{PD} + v_{OC})$. L_X therefore invests $E_{C(PD)}$ or $0.5C_{PZ}v_{PD}{}^2$ to later collect $E_{C(PK)}'$ at $0.5C_{PZ}(v_{PD} + v_{OC})^2$, so across that half cycle, i_{PZ} delivers with $E_{PZ(1/2)}'$ the difference:

$$\begin{aligned} E_{PZ(1/2)}' &= E_{C(PK)}' - E_{C(PD)} \\ &= 0.5C_{PZ}\left[\left(v_{OC}+v_{PD}\right)^2 - v_{PD}{}^2\right], \\ &= 0.5C_{PZ}\left(v_{OC}{}^2 + 2v_{OC}v_{PD}\right) \end{aligned} \quad (7)$$

which is $C_{PZ}v_{OC}v_{PD}$ higher than its unpre-damped counterpart. In other words, pre-damping C_{PZ} draws more energy from i_{PZ}.

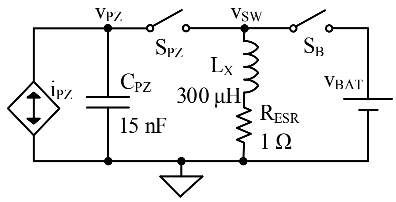

Fig. 3. Asymmetrically pre-damped piezoelectric charger [13].

IV. Asymmetrically Pre-Damping Charger

The charger in Fig. 3 from [13] pre-damps C_{PZ} for i_{PZ}'s negative half cycle, but not for i_{PZ}'s positive counterpart. In other words, like Fig. 2's gray trace shows, i_{PZ} charges C_{PZ} across i_{PZ}'s positive half cycle to charge C_{PZ} to v_{OC}. Battery switch S_B then closes to deposit some energy into L_X. After a short connection time, S_B opens and piezoelectric switch S_{PZ} closes for less than a quarter resonance period $0.25\tau_{LC}$ to drain C_{PZ} into L_X and another $0.25\tau_{LC}$ to deliver L_X's energy back to C_{PZ}, but in the negative direction. This way, C_{PZ}'s v_{PZ} first collapses to zero and then pre-charges to pre-damping voltage $-v_{PD}$.

Once at $-v_{PD}$, S_{PZ} opens and i_{PZ} charges C_{PZ} another v_{OC} in the negative direction to $-(v_{PD} + v_{OC})$. S_{PZ} then closes across $0.25\tau_{LC}$ to drain C_{PZ} into L_X, and after S_{PZ} opens, S_B closes until L_X depletes into v_{BAT}. In other words, the system invests $0.5C_{PZ}v_{PD}^2$ to pre-charge C_{PZ} to v_{PD} and collects $0.5C_{PZ}v_{OC}^2$ after C_{PZ} peaks to v_{OC} and $0.5C_{PZ}(v_{PD} + v_{OC})^2$ after C_{PZ} peaks to $-(v_{PD} + v_{OC})$ to draw $P_{PZ(A)}$

$$\begin{aligned} P_{PZ(A)} &= \left(E_{C(PK+)} - E_{C(PD)} + E_{C(PK-)}\right)f_{VIB} \\ &= 0.5C_{PZ}\left[v_{OC}^2 - v_{PD}^2 + \left(v_{PD} + v_{OC}\right)^2\right]f_{VIB} \\ &= C_{PZ}\left(v_{OC}^2 + v_{OC}v_{PD}\right)f_{VIB} \end{aligned} \quad (8)$$

A. Maximum Output Power

Since the system draws more power with higher pre-damping voltages, $P_{PZ(A)}$ peaks when v_{PD} is as high as possible. In the case of Fig. 3, v_{PZ} swings across overall damping voltage $v_{PZ(PP)}$ from v_{OC} to $-(v_{PD} + v_{OC})$, so C_{PZ} exposes S_{PZ} to this $v_{PZ(PP)}$. $P_{PZ(A)}$ therefore maxes when $v_{PZ(PP)}$ is near S_{PZ}'s breakdown level V_{BD}:

$$v_{PZ(PP)} = v_{OC} + \left(v_{PD} + v_{OC}\right) = 2v_{OC} + v_{PD} \le V_{BD} . \quad (9)$$

So when t_{VIB} is 10 ms, C_{PZ} is 15 nF, v_{OC} is 2 V, and V_{BD} is 20 V, v_{PD} should be 16 V for $P_{PZ(A)}$ to peak to 54 μW, which is 9× higher than $P_{PZ(0)}$'s unpre-damped 6 μW in Fig. 2.

With every energy transfer, however, the system loses ohmic and gate-drive power to the switches and ohmic power to L_X's R_{ESR}, but as mentioned earlier, mostly to R_{ESR}'s P_R. For instance, at the end of the positive half cycle, at 5 ms in Fig. 2, R_{ESR} burns power when v_{BAT} deposits energy into L_X, L_X drains C_{PZ}, and L_X pre-charges C_{PZ} to $-v_{PD}$. At the end of the other half cycle, at 10 ms, R_{ESR} similarly dissipates power when L_X drains C_{PZ} and then charges v_{BAT}. So in the end, v_{BAT} receives the difference between $P_{PZ(A)}$ and these R_{ESR} losses.

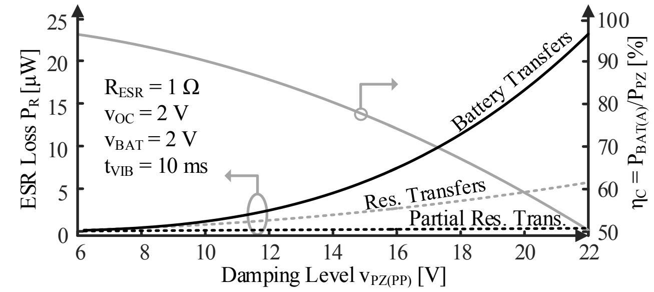

Fig. 4. Simulated ohmic conduction losses and power-conversion efficiency.

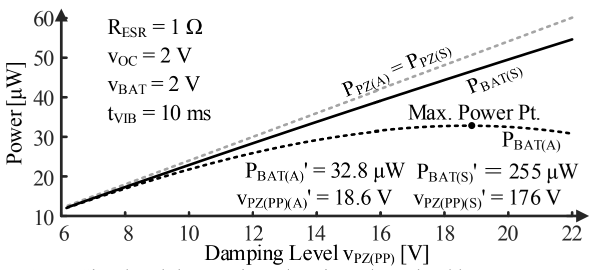

Fig. 5. Simulated drawn piezoelectric and received battery power.

All these losses climb with L_X's transfer energy $E_{L(PK)}$, and more specifically, with L_X's $i_{L(PK)}$. But of these, P_R for battery transactions rises more quickly (with $i_{L(PK)}^3$) than for capacitor transactions (with $i_{L(PK)}^2$). And since v_{BAT}'s investment energy rises with pre-damping voltage v_{PD}, battery-transfer losses climb with $v_{PZ(PP)}$ in Fig. 4 more quickly than for capacitor transfers. So much so that losses outpace $P_{PZ(PD)}$ gains in Fig. 5 when $v_{PZ(PP)}$ exceeds 18.6 V. In other words, output power into v_{BAT} peaks at $P_{BAT(A)}'$ when $v_{PZ(PP)}$ is 18.6 V, at which point v_{BAT} receives 33 of $P_{PZ(A)}$'s 50 μW when R_{ESR} is 1 Ω.

V. Symmetrically Pre-Damping Charger

The chargers in [5], [14]–[15] pre-damp C_{PZ} for both half cycles. Unfortunately, they either use multiple inductors, which occupy considerable space and consume substantial power, or v_{BAT} limits C_{PZ}'s pre-damping level. The charger proposed here in Fig. 6, on the other hand, is flexible enough with one inductor to pre-charge C_{PZ} to almost any value. Although similar to [6], the operation of this circuit is vastly different because this topology pre-damps C_{PZ} and the one in [6] does not. Note, by the way, D_N is in practice a switch that operates like a diode, so D_N drops millivolts when conducting.

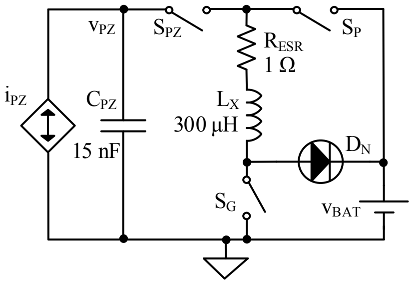

Fig. 6. Proposed symmetrically pre-damping piezoelectric charger.

Here, S_{PZ} and S_G close at the end of the positive half cycle across a quarter resonance period $0.25\tau_{LC}$ to drain C_{PZ} into L_X plus a fraction of that to start pre-charging C_{PZ}. S_G then opens and D_N steers L_X's i_L to v_{BAT} so C_{PZ} pre-charges to $-v_{PD}$ and v_{BAT} receives whatever energy remains. C_{PZ}'s v_{PZ} in Fig. 7 at 5 ms therefore collapses to zero and pre-charges to $-v_{PD}$.

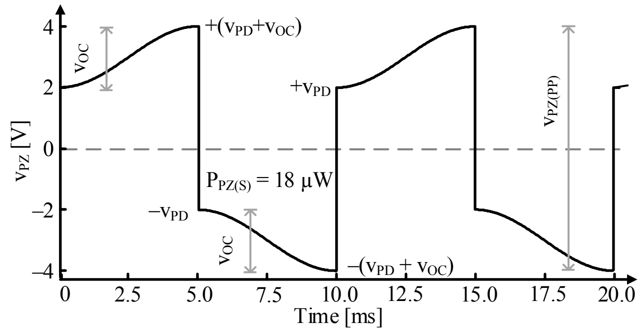

Fig. 7. Symmetrically pre-damped piezoelectric voltage.

i_{PZ} then charges C_{PZ} by v_{OC} across i_{PZ}'s negative half cycle to $-(v_{PD} + v_{OC})$. At that point, at 10 ms, S_{PZ} and S_G similarly close long enough to drain C_{PZ} into L_X, and at some point, S_{PZ} opens and S_P steers i_L to v_{BAT} to pre-charge C_{PZ} to $-v_{PD}$ and charge v_{BAT} with whatever energy remains. v_{PZ} at 10 ms therefore collapses to zero and pre-charges to $+v_{PD}$. After this, i_{PZ} charges C_{PZ} another v_{OC} across i_{PZ}'s positive half cycle to $v_{PD} + v_{OC}$, after which the sequence repeats. Like in the asymetrically pre-damped charger, $P_{PZ(S)}$ climbs with pre-damping voltage v_{PD}, but since C_{PZ} pre-charges before *both* half cycles, $P_{PZ(S)}$ delivers one more $C_{PZ}v_{OC}v_{PD}$ energy packet:

$$
\begin{aligned}
P_{PZ(S)} &= \left(E_{C(PK+)} - E_{C(PD-)} + E_{C(PK-)} - E_{C(PD+)}\right) f_{VIB} \\
&= 0.5 C_{PZ}\left[\left(v_{PD}+v_{OC}\right)^2 - v_{PD}^{\ 2} + \left(v_{PD}+v_{OC}\right)^2 - v_{PD}^{\ 2}\right] f_{VIB} \quad (10) \\
&= C_{PZ}\left(v_{OC}^{\ 2} + 2 v_{OC} v_{PD}\right) f_{VIB}
\end{aligned}
$$

A. Maximum Output Power

Since the system draws more power with higher pre-damping voltages, $P_{PZ(S)}$ peaks when v_{PD} is as high as possible. In the symmetrical case, v_{PZ} swings across $v_{PZ(PP)}$ from (v_{PD} + v_{OC}) to –(v_{PD} + v_{OC}), which means C_{PZ} exposes S_{PZ} to 2(v_{PD} + v_{OC}) and $P_{PZ(S)}$ maxes when $v_{PZ(PP)}$ is near S_{PZ}'s breakdown V_{BD}:

$$v_{PZ(PP)} = 2\left(v_{PD} + v_{OC}\right) \le V_{BD}. \quad (11)$$

So when t_{VIB} is 10 ms, C_{PZ} is 15 nF, v_{OC} is 2 V, and V_{BD} is 20 V, v_{PD} should be 8 V for $P_{PZ(S)}$ to peak at 54 μW, which matches $P_{PZ(A)}$'s asymmetrically pre-damped counterpart.

The system, however, loses power with every transaction mostly to R_{ESR}. So R_{ESR} burns power between every half cycle when L_X drains C_{PZ}, L_X pre-charges C_{PZ}, and L_X charges v_{BAT}. These losses climb with L_X's transfer energy $E_{L(PK)}$, and as a result, with L_X's $i_{L(PK)}$. Although P_R for battery transactions rises more quickly (with $i_{L(PK)}^{\ 3}$) than for capacitor transactions (with $i_{L(PK)}^{\ 2}$), v_{BAT} no longer invests energy to raise v_{PD}. As a result, battery-transfer losses in Fig. 8 climb with v_{PD} almost as quickly as for capacitor transfers. Still, P_R climbs faster than $P_{PZ(S)}$, and when $v_{PP(PZ)}$ surpasses 176 V, P_R outpaces $P_{PZ(S)}$ to peak output power $P_{BAT(S)}$' in Fig. 5 to 255 μW when R_{ESR} is 1 Ω. But 176 V is so high that V_{BD}'s 20 V, for example, limits $P_{BAT(S)}$ to 49 of $P_{PZ(S)}$'s possible 54 μW.

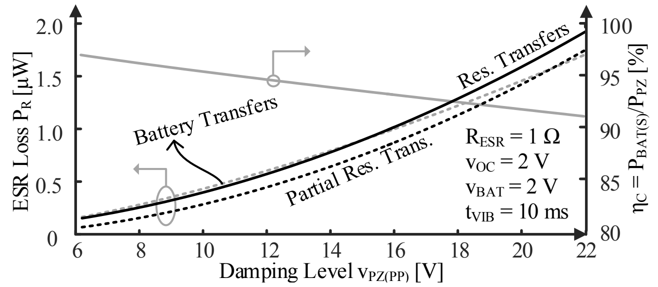

Fig. 8. Simulated ohmic conduction losses and power-conversion efficiency.

VI. Comparison

Although piezoelectric power P_{PZ} rises with pre-damping voltage v_{PD}, breakdown voltage V_{BD} limits C_{PZ}'s swing $v_{PZ(PP)}$, and in consequence, P_{PZ}. But since both pre-damping strategies can swing C_{PZ} by the same amount, P_{PZ} peaks to the same level. In other words, symmetrical and asymmetrical pre-damping strategies can draw the same piezoelectric power.

Transactions, however, consume power, so output power P_{BAT} into v_{BAT} does not always rise with the pre-damping level. In fact, battery transfers burn more power than capacitor transactions. And, ohmic power climbs quadratically or faster with peak inductor current $i_{L(PK)}$. So, since the asymmetrical case requires battery assistance to pre-damp C_{PZ}, the asymmetrical charger burns more power. The asymmetrical charger also transfers twice as much energy at the end of the cycle than the symmetrical charger does every half cycle. As a result, the symmetrical charger proposed burns 82% less and outputs 7.8× more power than the former from [11].

VII. Conclusions

Although the proposed symmetrically pre-damping charger and [11]'s asymmetrical counterpart can draw the same piezoelectric power, the proposed harvester can at 255 μW output 7.8× more power than [11] can at 33 μW with 1 Ω of ESR. Even when breakdown voltage is 20 V, the proposed circuit still outputs 46% more power. The basic reason for this improvement is lower ohmic losses. For one, the battery *only* receives power, whereas [11] both invests and receives. Plus, the battery receives two smaller packets instead of [11]'s one larger packet, so quadratic ohmic losses are lower. Since power and therefore losses fall with lower damping levels, these benefits diminish with lower breakdown voltages. Still, losses are nevertheless lower, and as a result, output power is higher, which is paramount for wireless microsensors.

References

[1] D. Puccinelli and M. Haenggi, "Wireless sensor networks: applications and challenges of ubiquitous sensing," *IEEE Circuits and Syst. Mag.*, vol. 3, no. 3, pp. 19–29, 2005.

[2] R.D. Prabha and G.A. Rincón-Mora, "0.18-μm light-harvesting battery-assisted charger–supply CMOS system," *IEEE Trans. on Power Electronics*, vol. 31, no. 4, pp. 2950-2958, Nov. 2015.

[3] S.P. Beeby, M.J. Tudor, and N.M. White, "Energy harvesting vibration sources for microsystem applications," *Meas. Sci. Technol.,* vol. 17, pp. R175–195, Dec. 2006.

[4] D. Guyomar, A. Dadel, E. Lefeuvre, and C. Richard, "Toward energy harvesting using active materials and conversion improvement by nonlinear processing", *IEEE Trans. Ultrason. Ferroelectr. Freq. Control*, vol. 52, no. 3, pp. 584–595, Apr. 2005.

[5] J. Dicken, P.D. Mitcheson, I. Stoianov, and E.M. Yearman, "Power-Extraction circuits for piezoelectric energy harvesters in miniature and low-power applications," *IEEE Trans. on Power Electronics*, vol. 27, no. 11, pp. 4514–4529, Nov. 2012.

[6] D. Kwon and G. A. Rincon-Mora, "A rectifier-free piezoelectric energy harvester circuit", *Proc. Inter. Symp. on Circuits and Syst*., pp. 1085–1088, May 2009 .

[7] M. Marzencki, Y. Ammar, and S. Basrour, "Integrated power harvesting system including a MEMS generator and a power management circuit," *Sensors and Actuators A: Physical,* vol. 146–146, no. 1-2, pp. 363-370, Jul./Aug. 2008.

[8] R.J.M. Vullers, R. van Schaijk, I. Doms, C. van Hoof, and R. Mertens, "Micropower energy harvesting," *Solid-State Electronics*, vol. 53, no. 7, pp. 684–693, Jul. 2009.

[9] S. Guo and H. Lee, "An efficiency-enhanced CMOS rectifier with unbalanced-biased comparators for transcutaneous-powered high-current implants," *IEEE J. Solid-State Circuits*, vol. 44, no. 6, pp. 1796–1804, June 2009.

[10] P. D. Mitcheson, T. C. Green, and E. M. Yeatman, "Power processing circuits for electromagnetic, electrostatic and piezoelectric inertial energy scavengers", *Microsystem Technologies*, vol. 13, no. 11, pp. 1629-1635, July 2007.

[11] D. Kwon and G.A. Rincón-Mora, "A 2-um BiCMOS Rectifier-Free AC-DC Piezoelectric Energy Harvester-Charger IC," *IEEE Trans. on Biomedical Circuits Syst.*, vol. 4, no. 6, pp.400–409, Dec. 2010.

[12] T. Umeda, H. Yoshida, S. Sekine, Y. Fujita, T. Suzuki, and S. Otaka, "A 950-MHz rectifier circuit for sensor network tags with 10-m distance," *IEEE J. Solid-State Circuits*, vol. 41, no. 1, pp. 35–41, Jan. 2006.

[13] D. Kwon and G.A. Rincón-Mora, "A single-inductor 0.35 um CMOS energy-investing piezoelectric harvester," *IEEE J. of Solid-State Circuits*, vol. 49, no. 10, Oct. 2014.

[14] J. Dicken, P.D. Mitcheson, I. Stoianov, and E.M. Yeatman, "Increased power output from piezoelectric energy harvesters by pre-biasing," in *Proc. PowerMEMS*, pp. 75–78, Dec. 2009.

[15] E. Lefeuvre, A. Badel, C. Richard, L. Petit, and D. Guyumar, "A comparison between several vibration-powered piezoelectric generators for standalone systems", *Sensors and Actuators A: Physical*, vol. 126, no. 2, pp. 405–416, Feb. 2006.